II. LITERATURE REVIEW

2.1 Structural developement during reheating stage

One of the consequences of reheating process is grain coarsening. The control of grain coarsening behavior of steel is an important step in the design of thermomechanical treatment to achieve fine grained products (1,2).

For microalloyed steels, the reheating temperaure should be high enough to provide solubility of stable particles. If the stable particles remain undissolved, the beneficial precipitation hardening effects can not be obtained. So it is necessary to know the solubility of stable or second phase particle.

2.1.1 Solubility relationships for precipitate products of titanium

Titanium has a strong affinity for oxygen and any titanium additions to a melt will be trapped as coarse TiO_2 particles unless the steel is fully killed with aluminium. The affinity of titanium nitride particles are useful if they are fine enough to restrain austenite grain growth on reheating and during hot rolling (3,4) . Several equations are aviable to describe TiN solubility (5,6,7,8). A more realistic result (9,10) using a.0.14 wt%c, 1.54% Mn,0.31% Si, 0.023% Ti, 0.0084% N steel , was obtained by Matsuda and Okumura (11).

$$\log [Ti][N] = \frac{-8000}{T} + 0.32 \qquad [1]$$

Where [Ti] and [N] are titanium and nitrogen solubility product respectively , and T is absolute temperature. Details are described in Fig. 2.1.

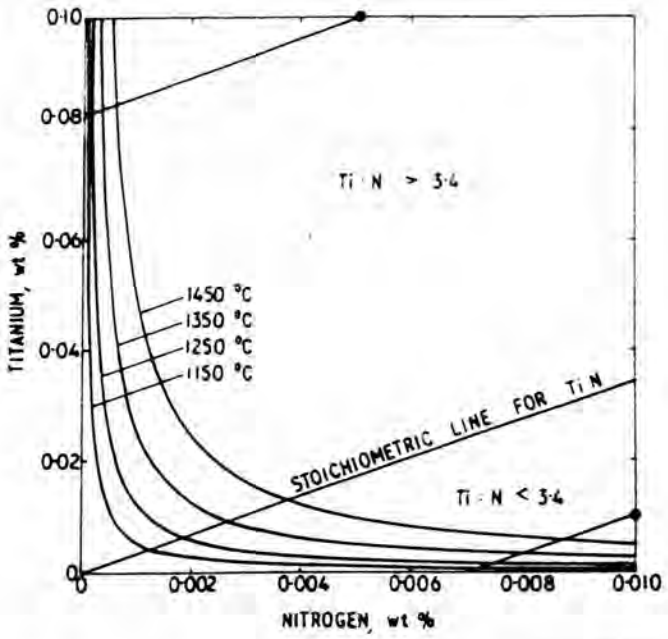

Fig. 2.1 Solubility of titanium nitride. Straight line show change in solute composition during precipitation.

After the titanium necessary for fixing nitrogen has been accounted for, the next stronger affinity is for sulphur (12). This action can be beneficial since if sufficient titanium is present, the normally highly deformable manganese sulphide inclusions are modified to become more resistant to deformation during hot rolling. Above 0.05 wt% Ti carbo-sulphide can also be produced. The stability of these sulphides is of the same order as for carbide , so that it depends critically on composition how much titanium is used as sulphide before carbide formation can take place. Irvine et al.(13) give the relationship of solubility of titanium carbide as follow

$$\log [Ti][C] = \frac{-7000}{T} + 2.75 \qquad [2]$$

Where [Ti] is residual wt% in solution.

2.1.2 Solubility relationships for precipitate products of niobium

The crystal structure of y-NbC_x can be represented by two interpenetrating fcc lattice with Nb atoms or Nb atom vacancies occupying the other set of lattice sites(14). The compound NbNy would likewise exhibit the same crystal structure. The compounds NbC_x and NbNy have complete solid solubility which enable them to form a carbonitride , NbC_xNy,

where x equals the atomic ratio C/Nb, y equals the atomic ratio N/Nb and 1-(x+y) equals the atomic ratio of vacancies (14). Henceforth NbC_x Ny will be referred to as Nb (CN).

The importance of Nb as a microalloying element in steel is apparent from the numerous studies performed over the past 30 years. Much of this work was concentrated on the solubility of NbC (14, 15, 27), NbN (14, 15, 16, 21, 24, 28, 29) and Nb (CN) (14, 15, 30-34) in austenite. The results of these studies are shown in Table 2.1 in the form of solubility product. The difference among these products are considerable and may be attributed to a number of reasons. Among these reasons is the variety of methods used in obtaining the given solubility, as each technique has its own assumptions and limitations. The techniques used in obtaining the solubility products of Table 2.1 are classified as A through E and are briefly described as follows:

(A) thermodynamic calculations,

(B) chemical separation and isolation of precipitate,

(C) equilibrating a series of steels with different Nb concentrations in a H_2 - CH_4 atmosphere at various temperatures, after which the C contents are analyzed,

(D) hardness measurements , and

(E) statistical treatment of existing solubility product.

Table 2.1 Solubility product for Nb-C , Nb-N and Nb-C-N systems in austenite

System	Product	Method	Reference
Nb-C	$\log [Nb][C] = 2.9 - 7500/T$	D	17
	$\log [Nb][C] = 3.04 - 7290/T$	B	18
	$\log [Nb][C] = 3.7 - 9100/T$	C	19
	$\log [Nb][C] = 3.42 - 7900/T$	B	20
	$\log [Nb][C] = 4.37 - 9290/T$	C	21
	$\log [Nb][C]^{0.87} = 3.18 - 7700/T$	B	22
	$\log [Nb][C]^{0.87} = 3.11 - 7520/T$	E	16
	$\log [Nb][C] = 2.96 - 7510/T$	E	16
	$\log [Nb][C]^{0.87} = 3.4 - 7200/T$	A	16
	$\log [Nb][C] = 3.31 - 7970/T +$ $[Mn](1371/T - 0.9) - [Mn]^2(75/T - 0.0504)$	B	23
	$\log [Nb][C]^{0.87} = 2.81 - 7019.5/T$	A	24
	$\log [Nb][C]^{0.87} = 3.4 - 7920/T$	C	25
	$\log [Nb][C] = 1.18 - 4880/T$	C	26
	$\log [Nb][C] = 1.74 - 5600/T$	C	27
	$\log [Nb][C] = 3.89 - 8030/T$	C	15
Nb-N	$\log [Nb][N] = 4.04 - 10{,}230/T$	C	29
	$\log [Nb][N] = 3.79 - 10{,}150/T$	B	22
	$\log [Nb][N] = 2.8 - 8500/T$	B	20
	$\log [Nb][N] = 3.7 - 10{,}800/T$	B	31
	$\log [Nb][N]^{0.87} = 2.86 - 7927/T$	A	24
	$\log [Nb][N] = 4.2 - 10{,}000/T$		28
Nb-C-N	$\log [Nb][C]^{0.24}[N]^{0.85} = 4.09 - 10{,}500/T$	B	16
	$\log [Nb][C + 12/14N] = 3.97 - 8800/T$	C	32
	$\log [Nb][C + N] = 1.54 - 5860/T$	B	16
	$\log [Nb][C]^{0.83}[N]^{0.14} = 4.46 - 9800/T$	B	16
	$\log [Nb][C + 12/14N] = 2.26 - 6770/T$	C	30

Thermodynamic calculation of solubility products often neglect any interaction between elements. As a result, the activity coefficients are assumed to be unity and the activities are represented by their weight percents. Recent work, however, has incorporated Wagner inter action parameters to account for the effect of alloying elements on the solubility of Nb (CN) in austenite (15,24). This lead to a more realistic solubility product since it incorporates nonunity activity coefficients.

The solubility data for the individual microalloy carbide and nitride (35) are shown in Fig. 2.2. It should be pointed out that there are significant differences in the published solubility product for a given alloy carbide or nitride but in general , the relative solubilities of various carbides and nitrides are as shown in Fig. 2.2

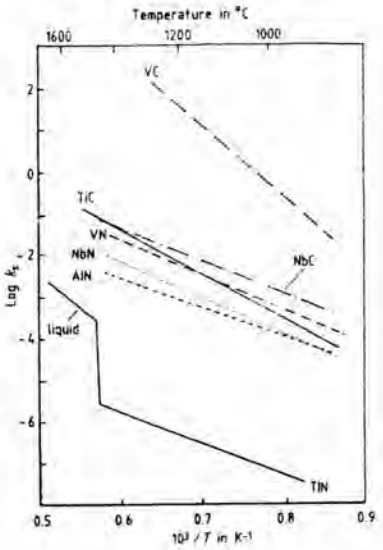

Fig. 2.2 Solubilities of microalloy carbides and nitrides

The solubilities of the nitrides are generally lower than those of the corresponding carbides, and this is paticularly true of titanium and vanadium where the difference in solubility betwen the nitride and carbide are paticularly pronounced. The solubilities of TiC, NbC, NbN, AIN and VN in austenite all tend to be very similar (within an order of magnitude) whereas the solubility of VC is much higher, by about two or three orders of magnitude, and the solubility of titanium nitride is same four orders of magnitude less.

2.1.3 Mutual solubility of titanium and niobium

Combined addition of microalloying elements (Nb and Ti) leads to formation of complex carbonitride precipitates , since the binary carbides and nitrides of such microalloying elements are mutually soluble (35). The formation of complex precipitates was reported in Nb-Ti (35, 37, 38) bearing steels, and the solubility of such particles depend on their composition. An example of complex precipitates formed in the 0.03% Nb-0.05% Ti steel which was reheated to 1200°C is shown in Fig. 2.3

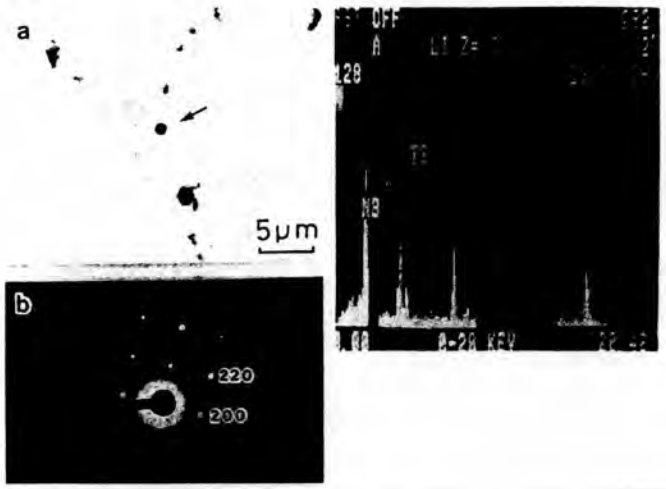

Fig. 2.3 (Nb-Ti) carbonitride precipitates in 0.03% Nb - 0.05% Ti steel reheated at 1150° C

The energy dispersive X-ray (EDX) spectrum from the particle (indicated by an arrow) shown in Fig. 2.3 (a) indicate the sharp peaks of both Nb and Ti while the electron diffraction pattern from the particle shown in Fig 2.3 (b) indicates the single crystal of B_1 structure. This suggests that Nb and Ti are mutually soluble in the precipitates, as previously reported (38).

Fig. 2.4 shows the microanalyzed composition for the precipitate particles and the amount of microalloys as precipitates in 0.028% Nb - 0.048% Ti and 0.027% Nb - 0.063% Ti steels reheat at temperatures between 900 and 1250°C. The composition of each precipitate particle was determined by scanning transmission electron microscope (STEM) - EDX and the amount of microalloys in precipitates was measured by means of chemical analysis of the electro-chemically extracted residue from the specimen (39).

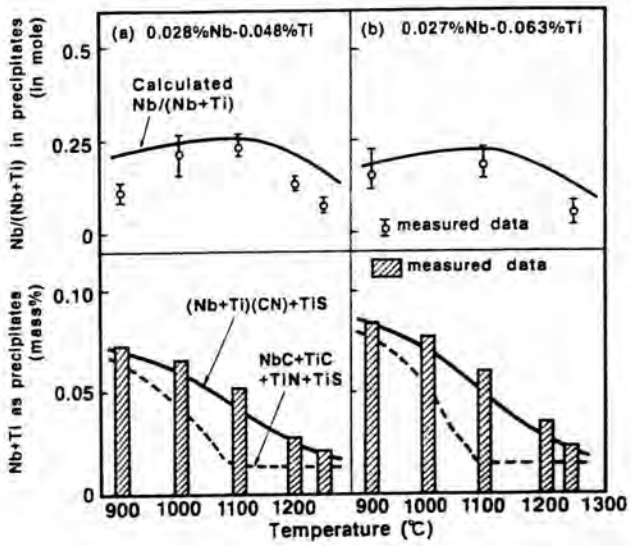

Fig. 2.4 Amount and composition of precipitates in Nb-Ti bearing steel reheated at various temperatures compared with calculated results from a (Nb, Ti,) (C,N) precipitation model

It is shown that the value of Nb/ (Nb + Ti) ratio varied from 0.1 to 0.3 with the peak at about 1100°C , and that carbonitride precipitate in Nb-Ti bearing steels are stable enough that more than 70% of microalloys in both steel are precipitated at about 1100°C. In Fig. 2.4 , calculated results for precipitation are also indicated. For the prediction of precipitation , two types of calculations were carried out. One was the Model for complex precipitates (Nb_x Ti_{1-x}) (C_y N_{1-y}) (39) (denoted by solid line) and the other was based on the independent precipitation (NbC + TiC + TiN) model by Keown and Willson (40) (denoted by broken line). For the estimate of the amount of Ti in precipitates, it was presumed that all titanium sulfides had already precipitated in Ti bearing steels. When comparing the calculated weights with measured weights of Nb + Ti as precipitate , the values calculated by independent precipitation model were much lower than the measured values in the steel or the values calculated by the complex precipitation model. This suggests that the mixing of Nb and Ti increases the stability of precipitates , so that the solubility of precipitates decreases in Nb-Ti steels through the formation of complex carbonitride.

2.1.4 Grain coarsening temperature of microalloyed steel

Addition of aluminuim , niobium, vanadium, titanium , etc., produces abnormal type of grain growth, as depicted in Fig. 2.5 , which involves the growth of very few grains in relatively unchanged fine-grain matrix. The abnormal grain growth occurs at the temperatures which are significantly lower than the microalloying solution temperature. The temperature that corresponds to commencing of the abnormal grain growth is sometimes referred to as grain coarsening tempereture (1).

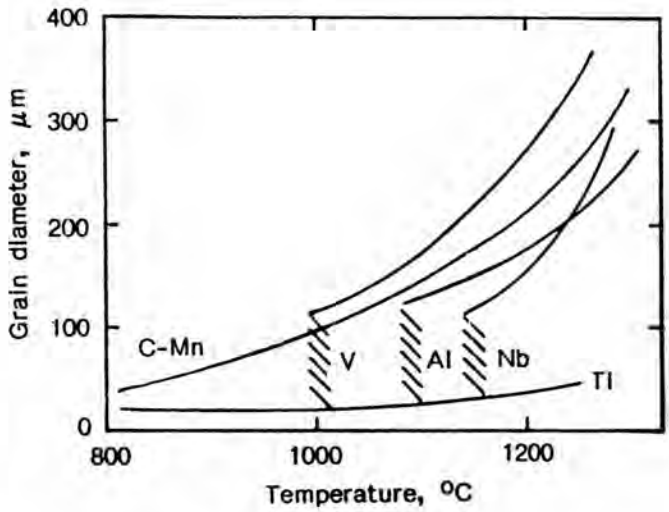

Fig. 2.5 Austenite grain coarsening characteristics in steels containing various microalloying addition.

The grain size distribution has a complicated dependence on the reheating temperature as depicted in Fig. 2.6 in application to Nb-V microalloyed steel. When reheating temperature is equal to 1200°C , the maximum area fraction of the steel microstructure corresponds to the grain size of approximately 120 micron. When the reheating temperature is lowered to 1150°C , the grain size occupying the maximum area fraction is reduced to 60 micron. However, further decrease in reheating temperature to 1050°C produce two pronounced peaks in distribution of the grain size , one of each is at the grain size of about 180 micron and the second one is at 22 micron (2).

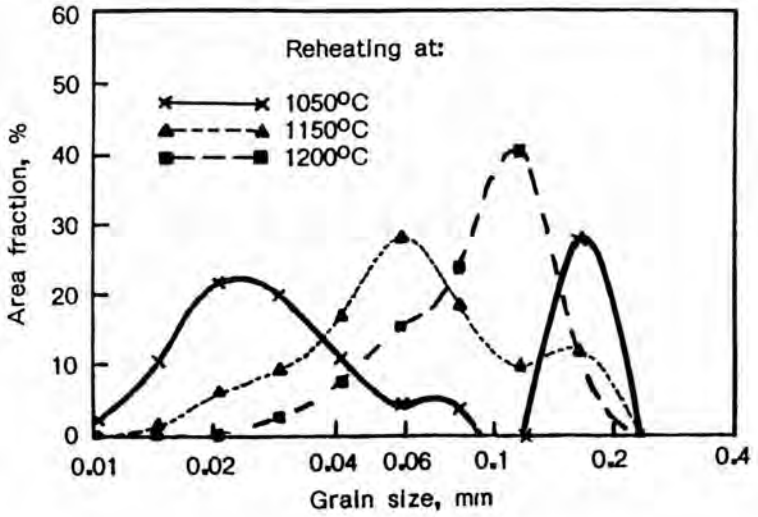

Fig. 2.6 Grain-size distribution in a Nb-V microalloyed steel after reheat 1 hour at three various temperature.

Abnormal grain coarsening occurs when the newly formed austenite grains are kept fine by the presence of a distribution of second - phase particles such as TiN, Nb (CN) , etc. Gladman (41,42) showed that there exists a critical condition where the energy release rate per unit displacement of grain boundary during grain coarsening is equal to the rate of energy release due to the absence of particle pinning. He defined this condition in terms of a critical particle radius, r_{crit}, which represents the maximum particle size that would effectively counteract the driving force for austenite grain coarsening

$$R_{crit} = \frac{6 R_o f}{\pi} \frac{(3 - 2)}{2 Z}^{-1} \qquad [3]$$

where , R_o is the initial matrix grain size, f is the volume fraction of particles, and Z is a term used to account for the heterogeneity of the matrix grain size.

It is clear from Eq [3] that for some given uniform initial grain size , r_{crit} will be the product of some constant and the particulate volume fraction of precipitate which will influence r_{crit}. This volume fraction will be sensitive to temperature as defined by the solubility relationship of precipitation compound. Therefore, as the temperature increase, progressively increasing amount of Ti, Nb, C and N go into solution in austenite (42,43). The result of this is that the volume fraction of second - phase particles available to retard grain coarsening

decreases. This situation leads to the coarsening of some grains at the expense of others, while some remaining grains continue to be pinned. Hence , a bimodal grain-size distribution develops that is clearly distinguished from the single grain-size distribution associated with normal grain coarsening.

Steels with typical compositions shown in Table 2.2 were determined for grain coarsening temperature.

Table 2.2 Chemical composition of steels.

Steel	C	P	Mn	Si	S	Al	Ti	Nb	V	N	Ca
A	.14	.018	1.00	.25	.012	.03	—	—	—	.005	—
B	.14	.018	1.00	.25	.012	.03	.015	—	—	.005	—
C	.13	.020	1.45	.40	.004	.03	—	—	—	.006	.0010
D	.13	.020	1.45	.40	.004	.03	.015	—	—	.006	.0010
E	.14	.020	1.40	.30	.010	.03	—	.025	—	.006	—
F	.13	.020	1.45	.40	.004	.03	.015	.025	—	.007	.0010
G	.12	.020	1.50	.40	.004	.03	.015	—	.045	.008	.0010

Results are summarised in Fig. 2.7 (44)

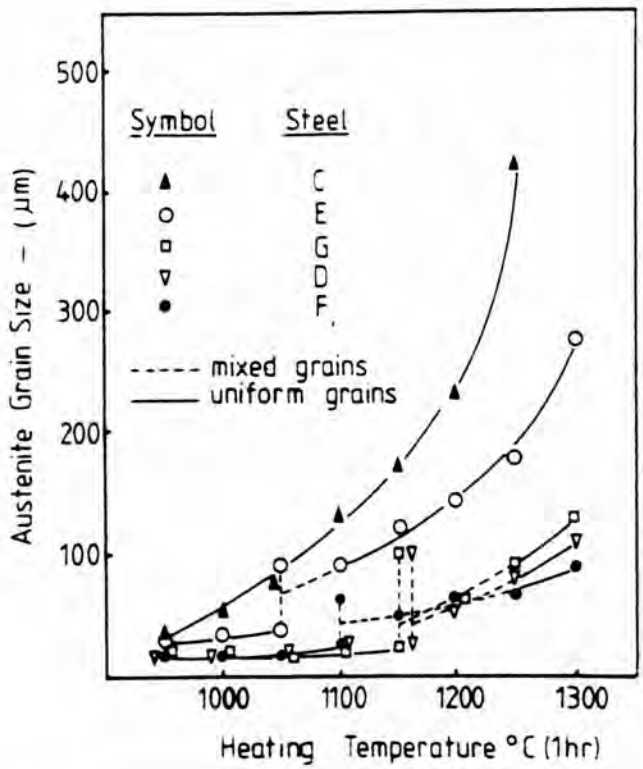

Fig. 2.7 Austenite grain growth in cast slab (1 hour at heating temperature)

As may be seen from a comparison of C-Mn steels C and D an addition of 0.01-0.02% Ti substantially increases the grain coarsening temperature. Furthermore, grain growth is greatly restricted in Ti treated steel D even after the onset of coarsening for heating temperature of up to 1300°C. At the grain coarsening temperature of steel D, abnormal grain growth occurs and mixed grains characteristically persist thereafter over a temperature range of about 100-150°C above the grain coarsening temperature. During this period the fine grained regions progressively diminish until relatively uniform coarser grains are usually observed at 1300°C. Very similar behaviour occurs for Ti treated C-Mn-Nb and C-Mn-V steels F and G respectively. A comparison of plain Nb steel E with Ti-Nb steel F in Fig. 2.7 also serves to demonstrate the significant grain growth control conferred by Ti especially at high reheating temperature.

2.2 *Deformation in recrystallization region*

The purpose of deformation in the austenite recrystallization region is to refine the austenite grain size as much as possible by repeated deformation and recrystallization. And it is well known that it is almost impossible to refine the austenite grain through dynamic recrystallization. Since the critical strain for the onset of dynamic recrystallization is very large, even at high temperature (45,46), grain refinement must be achieved by static recrytallization.

2.2.1 *Effect of the amount of deformation and deformation temperature on recrystallized grain size*

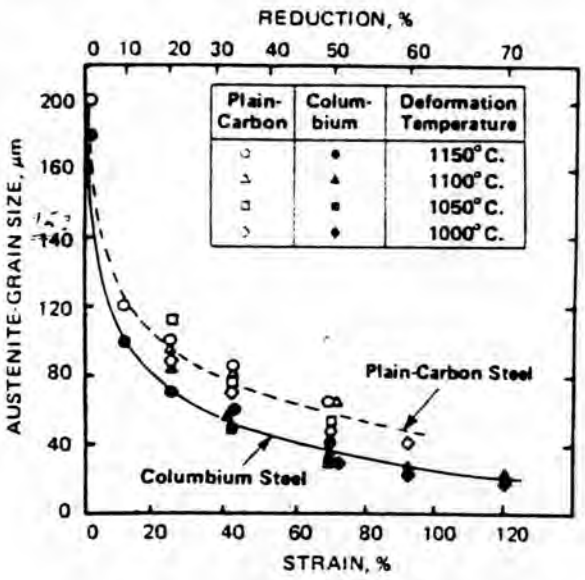

Fig.2.8 Influence of amount of single - pass deformation and deformation temperature on recrystallized austenite grain size

As shown in Fig. 2.8 the recrystallized grain size decreases with reducing initial grain size (48). Although a lower deformation temperature produce smaller grain sizes, the effect of temperature is slight.

2.2.2 *The critical amount of deformation (R_{crit})*

It must be stressed that static recrystallization in hot deformation does not occur under all conditions. On the contrary, it is necessary to apply more deformation than that required for recrystallization. The critical amount of deformation (R_{crit}) is small in plain cabon steel. In Nb steel, however, R_{crit} is very large and its temperature dependence is higher than in plain carbon steel (47). The effect of deformation temperature and initial grain size on Rcrit are shown in Fig. 2.9

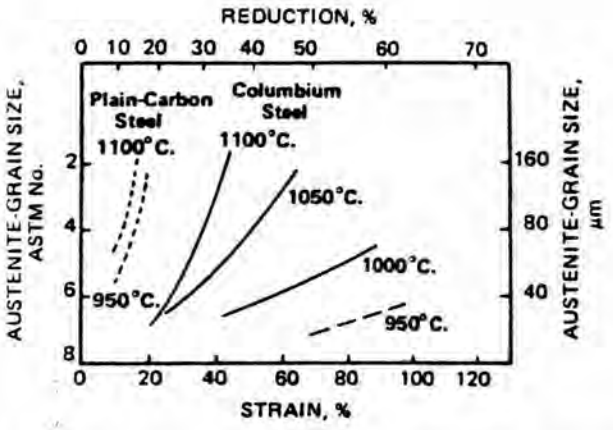

Fig. 2.9 Effect of deformation temperature and initial grain size on critical amount of deformation.

In Nb Steel , the effect of grain size on R_{crit} is extremely large , and R_{crit} increase rapidly with decreasing deformation temperature. Recrystallization is virtually suppressed below 950°C.

Ouchi et al (49) studied the general recrystallization behaviour by single-pass rolling , shown in Fig. 2.10. Recrystallization behaviour is divided into three regions, recovery , partial recrystallization region, and recrystallization. The recrystallization is subdivided into static and dynamic.

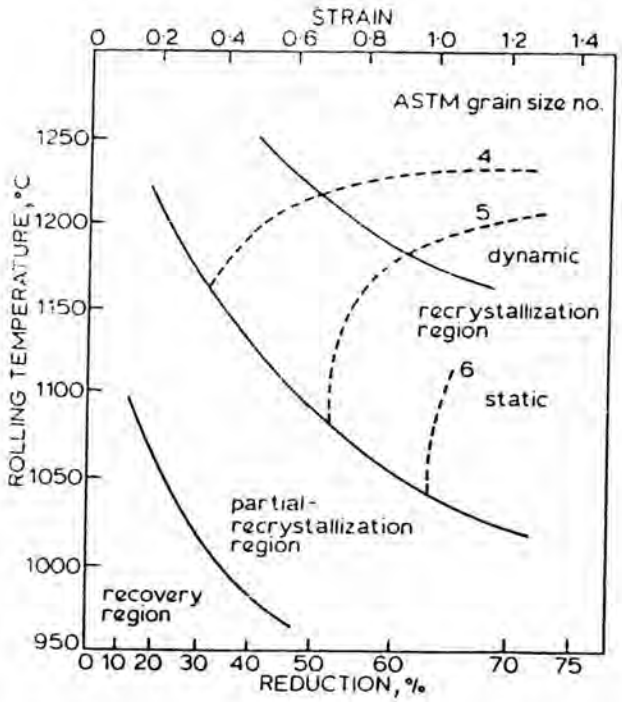

Fig. 2.10 Austenite recrystallization and resulting grain size as function of rolling temperature and reduction for 0.03% Nb steel.

The critical amount of deformation dividing each region increases rapidly with decreaseing deformation temperature. Reduction in the recrystallization produce a fine uniform recrystallization grain structure. Reduction in partial - recrystallization region produces a mixed structure consisting of recrystallization grains and recovered grain. Reduction in th recovery region produces locally very coarse grains due to strain-induced grain-boundary migration. While most grains remain unchanged, stored energy is released by recovery.

2.2.3 Recrystallization of Nb-Ti microalloyed steel

Fig. 2.11 shows the result of the single-pass rolling experiments of 0.065%C, 13%Mn , 0.2% Si , 0.027% Nb , 0.01% Ti, 0.005% N, <0.05% and P. (50).

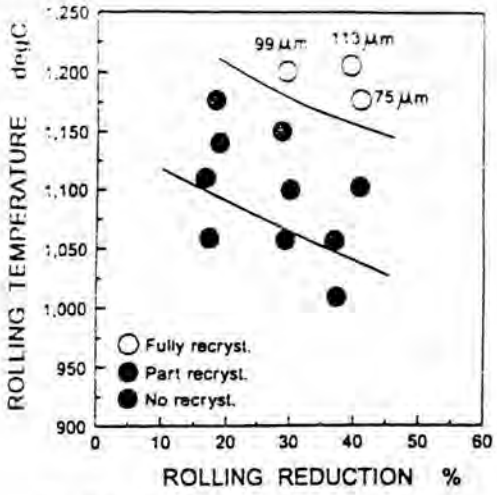

Fig. 5 Results of 1-pass rolling experiments.

Fig. 2.11 Results of 1 pass rolling experiment

There are three distinct regions in the figure:

(i) Combinations of rolling reduction and temperature which failed to cause any recrystallization,

(ii) Combinations which resulted in partial recrystallization ,

(iii) Combinations , at high temperature which caused complete recrystallization.

Fig. 2.12 illustrates partial and full recrystallization

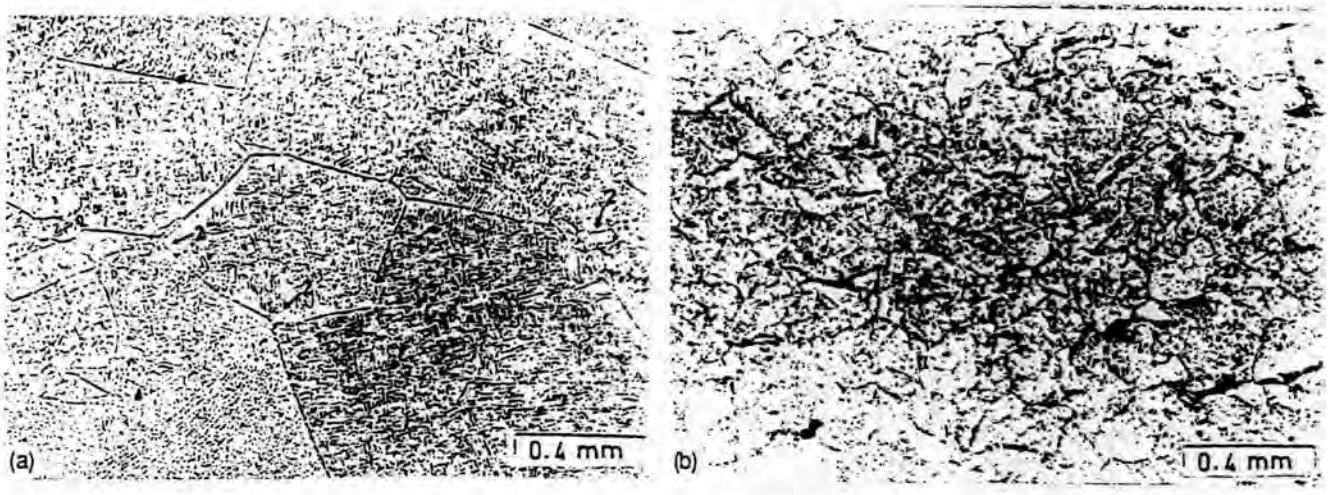

Figure 2.12 Austenite grain structure after rolling

(a) Start of recrystallization 16.4% Reduction at 1100°C

(b) Fully recrystallized - 39.2% reduction at 1200°C

Recrystallization started at grain corners and grain surfaces, corners being particularly favoured. The grain sized of fully recrystallized austenite are indicated in Fig. 2.11. It has

been suggested (51) that the grain size of statically recrystallized grains, DRX is related to original grain size , d_o and rolling strain , ε according to

$$D_{rx} = 1.1\ (d_o/\varepsilon)^{2/3} \qquad [4]$$

2.2.4 Recrystallization stop temperature (T_{rx})

As the rolling temperature decrease , recrystallization temperature becomes more difficult and reaches a stage where it effectively ceases. Cuddy (52) has defined the recrystallization stop temperature as the temperature at which recrystallization is incomplete after 15 seconds, after a particular rolling sequence. Using this criterion, the effect of common micro-alloying elements on recrystallizaiton behaviour is shown in Fig. 2.13

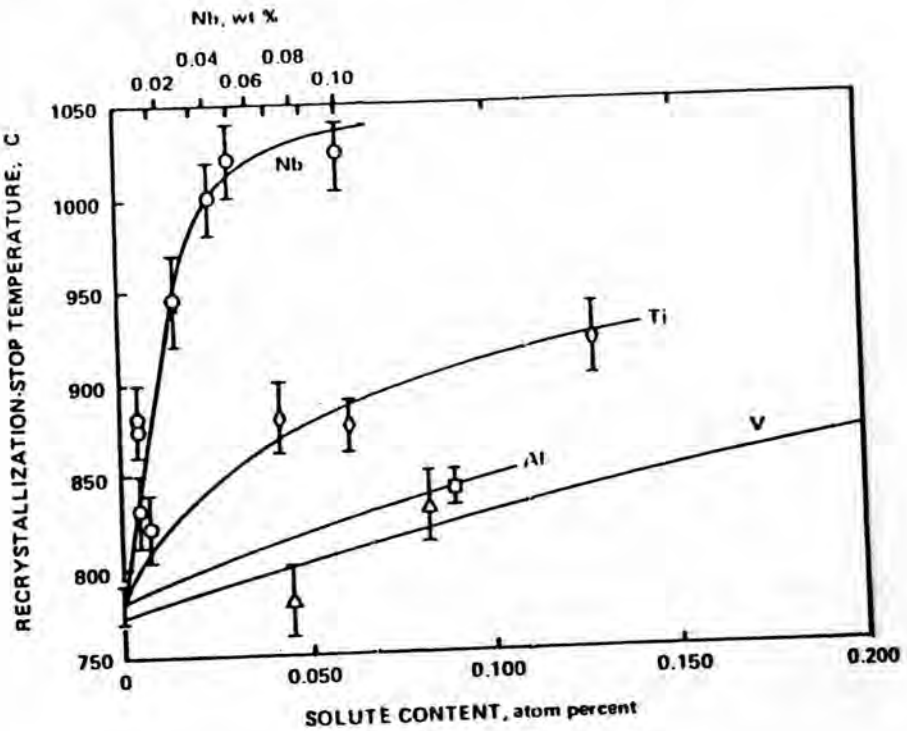

Fig. 2.13 Effect on recrystallization stop temperature of increase in microalloy content in 0.07% C, 1.4% Mn, 0.25%Si steel

Karjalainen et al (53) investigated for T_{rs} of steels that chemical composition are given in Table 2.2

Table 2.2 Chemical composition of studied steels

Grade	C	Mn	Nb	Ti	V	Al	Ni	N
Nb	0.081	1.46	0.041	0.001	0.005	0.041	0.03	0.005
Nb-Ti	0.090	1.51	0.033	0.015	0.008	0.041	0.03	0.006
Nb-Ti-V	0.050	1.46	0.041	0.015	0.082	0.050	0.03	0.009
Nb-Ti-Ni	0.071	1.57	0.041	0.018	0.006	0.034	0.70	0.005
low Nb-Ti	0.046	1.51	0.011	0.020	0.007	0.031	0.04	0.008
high Ti-Nb	0.076	1.20	0.046	0.142	*	0.034	0.03	0.003

Si 0.2-0.3 * Mo 0.1

Mean flow stress (MFS) are plotted against the inverse of absolute pass temperature , 1/T. This type of plot can be used to determine two of the critical temperatures of hot rolling : the recrystallization stop temperature, T_{rs}, and the start of the austenite-to-ferrite transformation temperature Ar3 (54,55). Details are shown in Fig. 2.14

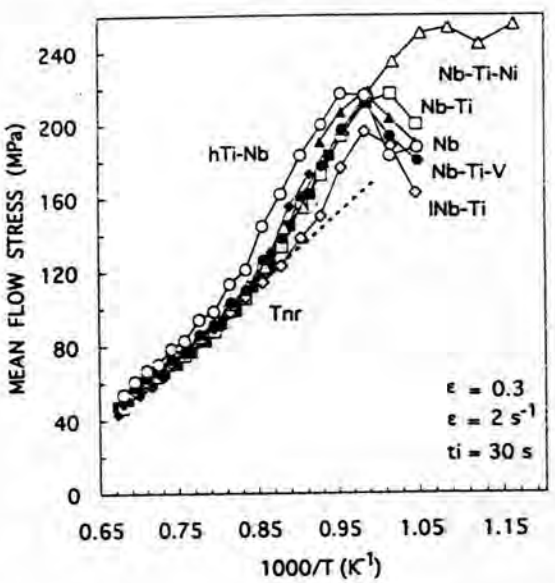

Fig. 2.14 MFS VS the 1/T curves for plate rolling simulation

The main results are listed in Table 2.3 where they are compared with the predictions of the empirical equations based on chemical composition reported by Barbosa et al (56) for T_{ni} (or T_{rs}) and by Ouchi et al (57) for Ar3.

Table 2.3 Measured and calculated no recrystallization (T_{nr}) and transformation start (Ar3) temperature (°C)

Grade	T_{Nr} meas.	T_{nr} calc.*	A_{r3} meas.	A_{r3} calc.**
Nb	945	980	755	766
Nb–Ti	925	956	760	759
Nb–Ti–V	935	990	770	774
Nb–Ti–Ni	915	945	705	718
low Nb–Ti	860	841	740	772
high Ti–Nb	960	1135	780	780
high Ti-Nb ($=0.2s^{-1}$)	985			

* $T_{nr}=887+464C+(6445Nb-644\sqrt{Nb})+(732V-230\sqrt{V})+890Ti+363Al-357Si$

** $A_{r3}=910-310C-80Mn-20Cu-15Cr-55Ni-80Mo$

2.3 Deformation in nonrecrystallication region

The purpose of deformation in the nonrecrystallization region is to increase ferrite-nucleation sites by producing deformation band in the interiors of elongated austenite grains. Fig. 2.15 depicts the transformation behaviour and resulting grain structure in hot-rolled and heat-treated steel(58)

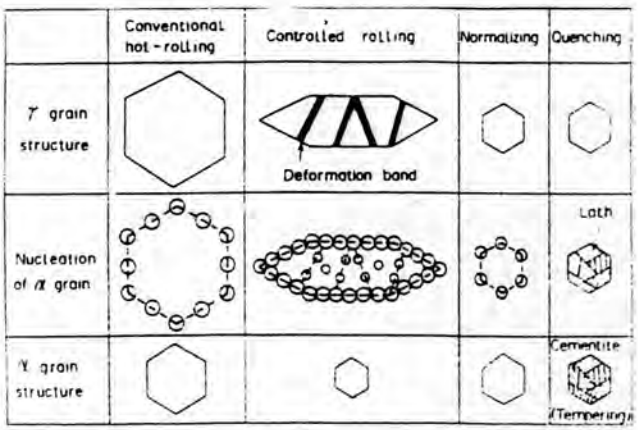

Fig. 2.15 Nucleation sites for ferrite grains and resulting ferrite grain structures in hot rolled and heat-treated steel.

The fundamental difference between conventionally hot rolled steel and controlled rolled steel lies in that, in the former ferrite grains nucleate exclusively at austenite grain boundaries, whereas in latter nucleation occurs in the grain interiors as well as grain

boundaries. Ferrite nucleation frequency is larger at deformed austenite grain boundaries than at recrystallized ones and that isolated ferrite nucleation occurs in the interiors of deformed austenite grains (59,60). These effects lead to a large different in the final ferrite grain structure in the two steel. The fact that the deformation band is equivalent to austenite grain boundary with regard to ferrite nucleating potential implies that an austenite grain is divided into several blocks by deformation bands. The difference in ferrite nucleation behaviour between conventionally hot rolled and controlled rolled steels is similar to that between normalized and quenched steels. In normalized steel, ferrite nucleation occurs exclusively at austenite grain boundaries, whereas in quenched steel austenite grain are divided into several blocks by martensite transformation. Besides quenching, it is only controlled rolling that can divide austenite grains, though the operating mechanism is quite different in this two cases (61)

2.3.1 Formation of deformation band

The nature of deformation bands is not known exactly, they generally exist in closely packed pairs of parallel lines which often terminate within a grain , creating a twin-like pattern in heterogeneous distribution(62). As shown in Fig. 2.16 deformation band density increase a little in a strain range of less then 30% , beyond which it increases rapidly with increasing reduction

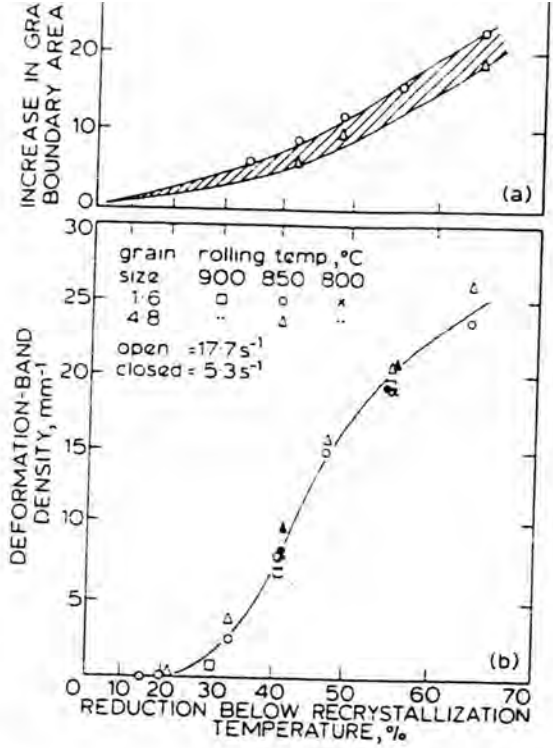

Fig. 2.16 Variation in austenite grain-boundary area and introduction of deformation bands resulting from reduction in nonrecrystallization region.

It can be seen that , with an increasing amount of reduction , the austenite grain boundary area increase gradually, while deformation band density increases rapidly, indicating that austenite grain refinement resulting from deformation in the nonrecrystallization region is due mainly to an increase in the deformation band. The grain boundary area is increased only by a factor of about 2 when total deformation in the nonrecrystallization region is 70-80% (63). It is also important to note that even when the deformation band is saturated in number, about 10% of austenite grains contain very few deformation bands (64) , and that not all deformation bands have the same ferrite nucleation potential (62) , some bands only have very thin straight bands of ferrite, implying poor nucleation capacity. Even the introduction of deformation bands cannot bring about uniform and homogeneous austenite grain structure and thereby homogeneous ferrite grain structure. Inhomogeneity in grain structure can be reduced with a decrease in recrystallized austenite grain size before deformation in the nonrecrystallization region.

The ferrite grain size correlating with effective austenite interfacial area Sv (grain boundary area plus deformation bands) are shown in Fig. 2.17

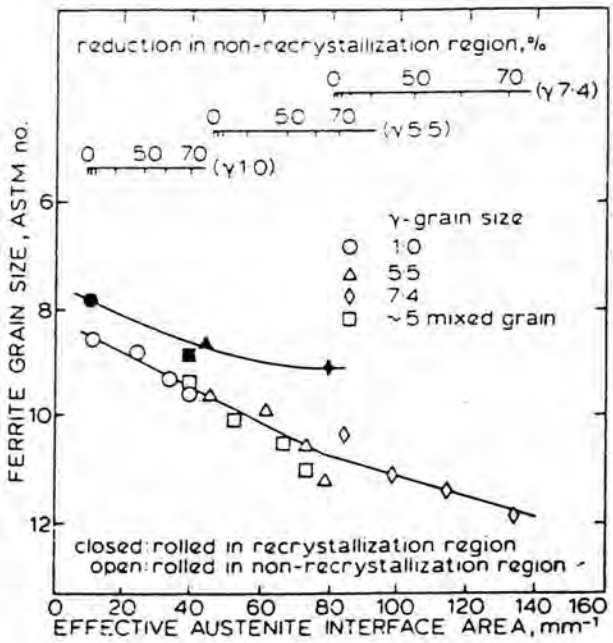

Fig. 2.17 Variation in ferrite grain size with effective austenite interface area in Nb (65)

Although an increase in Sv causes ferrite grain refinement , for a fixed Sv value deformation in the nonrecrystallization region refines ferrite more effectively than that in the recrystallization region. According to Ouchi et al (49), in the early stage of transformation the transformation rate is given by Ns x Sv , where Ns is the nucleation rate per unit boundary area. While austenite grain refinement through recrystallization increases only the Sv value , deformation in the nonrecrystallization region increase both Ns and Sv, because the unrecrystallized austenite structure contains a high dislocation density and substructure beside elongate grain boundaries and deformation bands, which surely enhance the nucleation rate Ns.

Fig. 2.18 (59) Depicts various nucleation sites for pearlite transformation in tool steel which was rolled 30% in the nonrecrystallization region

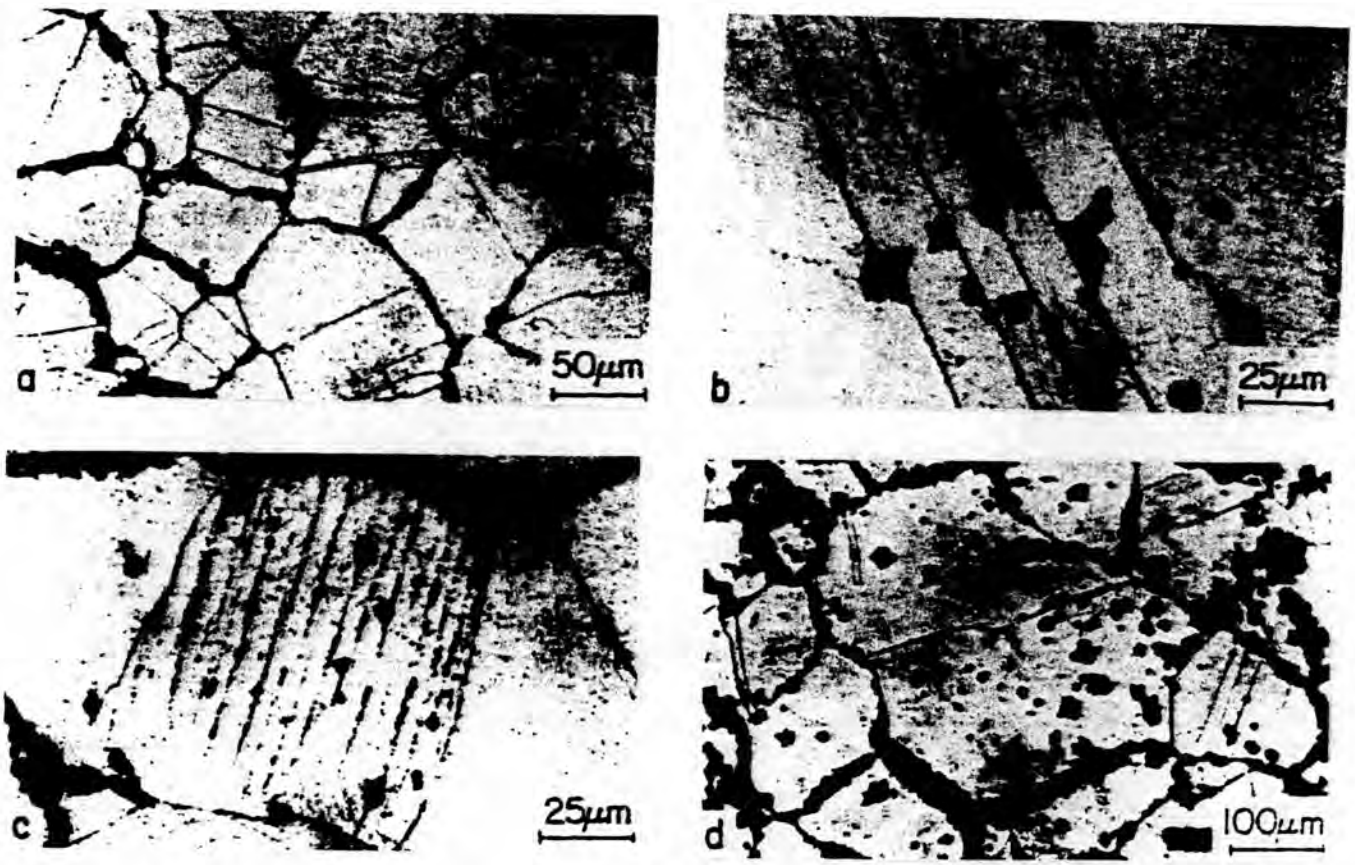

Fig. 2.18 Optical micrographs showing various types of nucleation sites for pearlite observed in deformed tool steel

(a) In the initial stage of transformation, pearlite nucleation occurs preferentially at grain boundaries,

(b) with the progress of transformation , pearlite nucleation occurs at annealing twin boundaries as well as austenite grain boundaries

(c) pearlite forms at deformation bands, and

(d) pearlite nucleation occurs in the interiors of grains.

In summary, the deformed specimen annealing twin boundaries and deformation bands were observed to act as the additional nucleation sites, and also the intragranular nucleation was observed beside the nucleation at austenite grain boundaries.

2.3.2 Effective nucleation area (Sv)

According to various authors (57,58,62,66,67,68) the common characteristic allowing mathematical description of the state of austenite before phase transformation is the expression of the effective nucleation area, Sv (mm^{-1}) which characterizes the equivalent area (mm^2) per unit volume. Kozasu (62) defined Sv as quantitative characterization of the number of potential ferrite nucleation in hot rolled austenite. According to Umemoto et al (69) the effective nucleation area of the grain boundaries of equiaxed nondeformed austenite grains can be expressed as follows

$$Sv\ (gb) = \frac{200}{d_\gamma} \quad (mm^{-1}) \qquad [5]$$

Where d_γ (um) is the diameter of the recrystallized austenite grain.

For the deformed austenite grain, Ouchi et al (57) express the effective nucleation area of the grain boundaries (gb) and the deformation bands (db) which are formed inside the deformed austenite grain as follows (69).

$$Sv\ (gb+db) = 0.429\ (N_L)_{//} + 1.571\ (N_L)\perp \quad (mm^{-1}) \qquad [6]$$

Where $(N_L)_{//}$, $(N_L)\perp$ are number of intersections on the unit of length parallel and perpendicular to the largest dimension of the deformed grain.

Providing that the number of intersections of grains and deformation bands (N_L) is measured on the length of 100 mm. and the microsopy magnification (z) is known, equation (6) will be rewritten as follow.

$$Sv\ (gb+db) = (0.429\ N_{L\,//}.z + 1.571\ N_L\perp.z)\ 10^{-2} \quad (mm^{-1}) \qquad [7]$$

The total effective nucleation area can be expressed as the sum of the effective nucleation area of the boundaries of austenite grains, Sv (gb) , and deformation bands, Sv (db) , i.e.

$$Sv\ (gb+db) = Sv\ (gb) + Sv\ (db)\ \ (mm^{-1}) \qquad [8]$$

2.3.3 The axes of deformed austenite

When a uniaxial recrystallized austenite grain is entering the plastic deformation then for simplicity we can substitute it by a circle having the diameter dx. Then this austenite grain will be deformed with ε_1 reduction. And after the plastic deformation no recrystallization of the material is assumed. As a result the circle is deformed to ellipe as depicted in Fig. 2.19

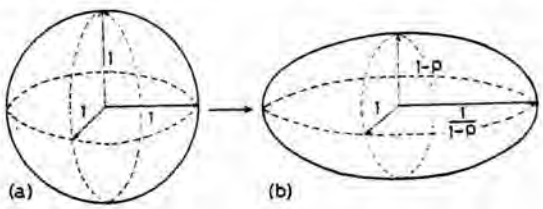

(a) Before rolling (sphere)
(b) After rolling (ellipsoid)

Fig. 2.19 The shape change of an austenite grain by reduction in nonrecrystallization region

The dimension of the ellipse grain are expressed as the function of deformation (70) :

- The major axis that parallel to the rolling direction

$$d_\gamma // = d_\gamma / (1- \varepsilon_1) \qquad [9]$$

- The conjugate axis that perpendicular to rolling direction

$$d_\gamma \perp = d_\gamma . (1- \varepsilon_1) \qquad [10]$$

The equations above come from calculation by applying statistical method. But when the calculation of axes of the deformed austenite grain were based on the experimental results where the length of the axes were determined from the equations:

$$d_\gamma // \ (gb+db)\ exp = \frac{1000.\ 100}{z\ n_L //} \quad (um) \qquad [11]$$

$$d_\gamma \perp (gb+db)\,exp = \frac{1000.\ 100}{z\ n_L \perp} \quad (um) \qquad [12]$$

Where "exp" denotes the experimental values.

2.3.4 The effect of rolling reduction on the grain boundary surface area

The surface area of austenite per unit volume increases by elongation of grains for simplicity, assume that the nitial austenite grain are spherical with unit radius as shown in Fig. 2.20(a). By applying the rolling with reduction P their shape becomes ellipsoid as shown Fig. 2.20 (b). The grain surface of grain before rolling is given as (59).

$$S^{o}gb = 4p$$

The surface area of a grain after rolling to reduction P is given as

$$Sgb\,(P) = \int_{-1/1-P}^{1/1-P} \left[\left\{ 4X \int_{0}^{\pi/2} (1-(2P-P^2)\sin^2 Q)^{1/2}\, dQ \right\} \times (X^2 (1-P)^6 + 1)^{1/2} \right] \frac{dX}{1-X^2 (1-P)^2} \qquad [14]$$

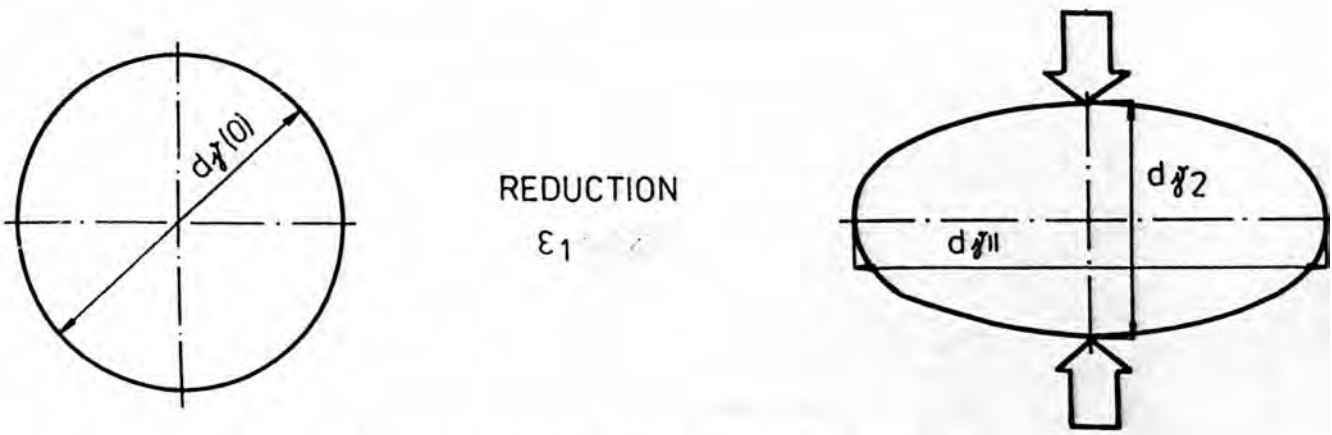

Fig. 2.20 The shape change of an austenite grain by the rolling with reduction P

The ratio of the surface area before rolling to that of after , q (= $S_{gb}(P)/S^{o}_{gb}$), is plotted in Fig. 2.21 as a function of rolling reduction P and true strain ε .

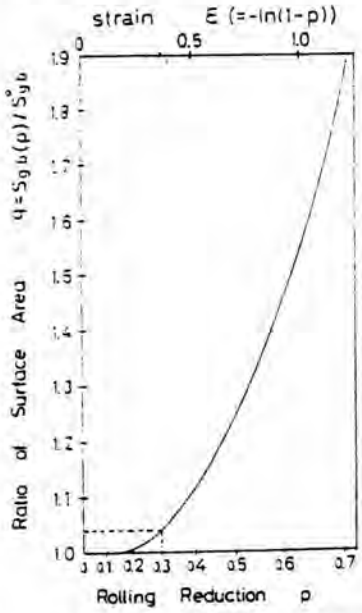

Fig. 2.21 The ratio of austenite grain surface area before rolling to that of after as a function of rolling reduction P.

Since the volume of sphere shown in Fig. 2.21 (a) is equal to that of ellipsoid shown in Fig. 2.21 (b) , the ratio q in Fig. 2.22 is equal to that pertaining to grain surface area per unit volume before and after rolling. It is seen that the increase in the grain surface area per unit volume with the increase in P is quite small when P is small (such as 30% reduction). At p=0.3 q is equal to 1.04

2.3.5 The mechanism of transformation acceleration by deformation

Umemoto et al (59) showed that plastic deformation in the austenite condition led to marked acceleration of transformation. Microscopic examination revealed that there was no detectable change in the growth rate by deformation. Thus it can be said that the acceleration of transformation is caused mainly by the increase in nucleation rate. The increase in nucleation rate per unit volume by deformation in austenite condition is considered to be attributed to the following three factors:

1) The increase in austenite grain surface area per unit volume by elongation of grains,

2) The increase in the nucleation rate per unit area of austenite grain surface, and

3) Formation of additional nucleation sites such as deformation bands

These three factors are illustrated seperately in Fig. 2.23

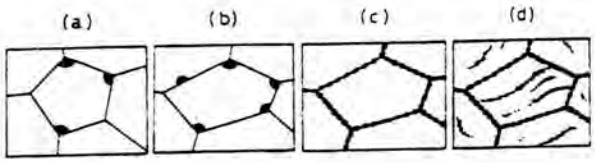

Fig. 2.22 An early stage of transformations in 4 different austenite conditions

In Fig. 2.22 an early stage of pearlite transformation in each austenite condition is drawn schematically to express the difference in austenite conditions clearly (a) shows the initial, non-deformed condition (b) shows a deformed condition in which the grain are elongated but nucleation rate per unit area of grains boundary is not altered and deformation bands are not produced (c) shows a deformed condition in which grains are elongated and nucleation rate per unit area of grain boundary is increased but deformation bands are not produced , and (d) shows a deformed condition where grains are elongated, nucleation rate is increased and deformation bands are produced on which to invite further nucleation.

Fig. 2.23 shows the ferrite grains nucleated on the austenite grain boundaries in the non-deformed (a) , 30%rolled (b)and 50%rolled (c) specimens, respectively (71)

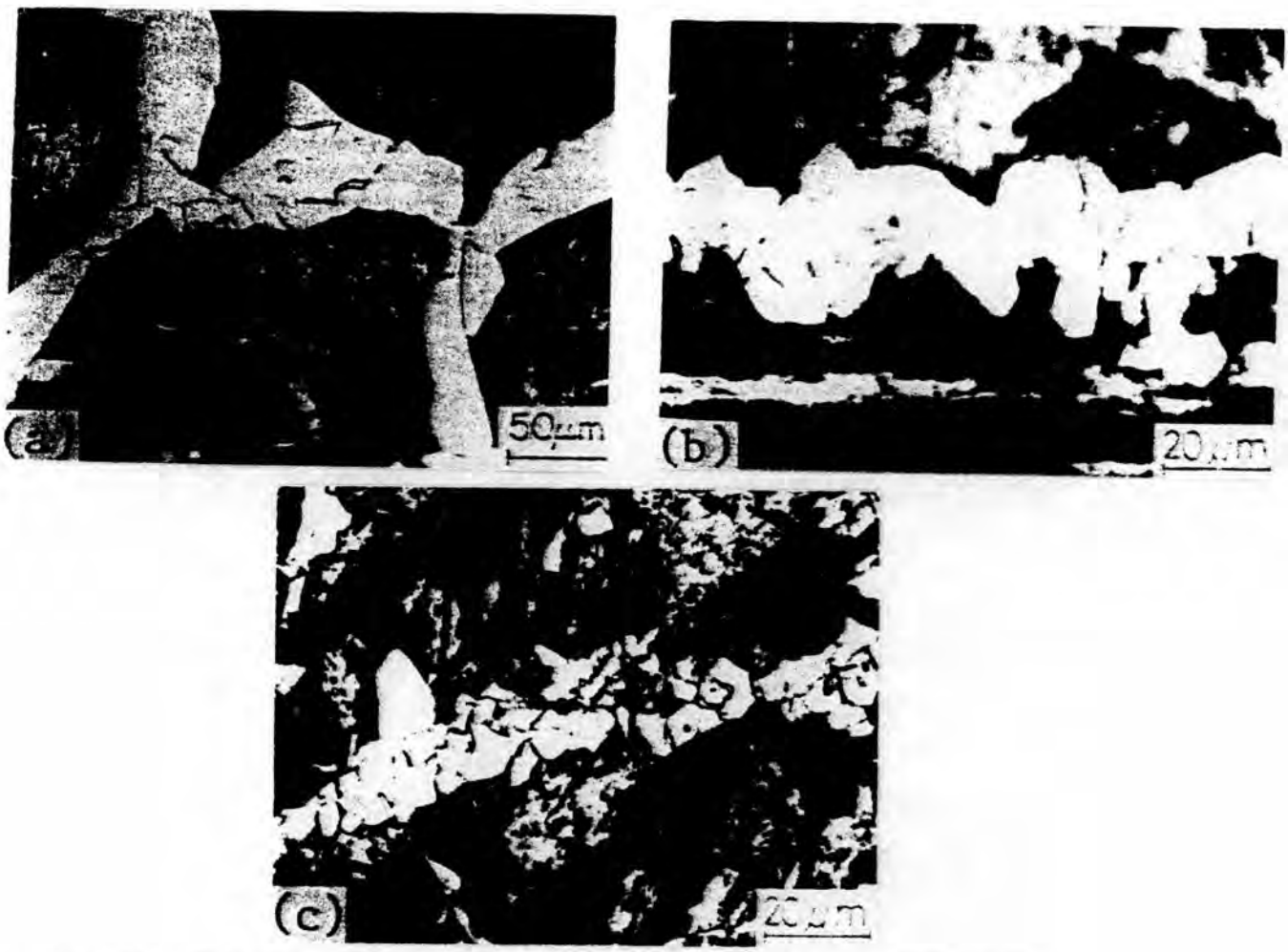

Fig. 2.23 Optical micrographs showing the effect of deformation on the number of ferrite grains formed at the austenite grain boundaries.

(a) not deformed , 3 min. at 680°C

(b) 30% rolled , 30 sec. at 680°C

(c) 50% rolled , 30 sec. at 680°C

It is seen that the number of ferrite grains nucleated on the austenite grain boundaries are substantially increased with the increase in the degree of deformation. From these picture the nucleation rate on the austenite grain boundaries was estimated. The number of ferrite

grain intercepts per 1 mm. of austenite grain boundry was counted as 41, 214 and 330 for 0, 30 and 50% rolled specimens respectively. The number of ferrite grains nucleated per unit area of austenite grain boundary surface is proportional to the square of these numbers. Furthermore, the number of ferrite grain nucleated per unit area of austenite grain surface when the grain boundaries are completely occupied by ferrite grains can be expressed as (70)

$$Ns = \sqrt{I} / (3/\sqrt{2}\,\alpha) \qquad [15]$$

Where I is the nucleation rate of ferrite per unit area of austenite grain surface and α is the parabolic rate constant. Thus the ferrite nucleation rate per unit area of the austenite grain boundary surface was estimated to be increased by 740 ($(214/41)^4$) and 4200 ($(330/41)^4$) times for 30% and 50% rolling.

2.3.6 Effect of deformation below recrystallization Temperature (Tnr) of Austenite on Transformation Temperature (Ar_3)

Ouchi et al (57) studied effect of deformation below Tnr on Ar_3 , result as depicted in Fig. 2.24. The investigated steel composition was 0.16%C, 0.36%Si, 1.41% Mn and 0.031% Nb.

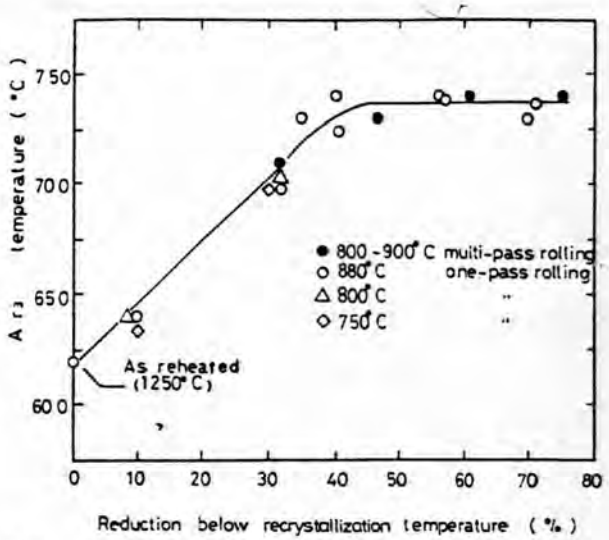

Fig. 2.24 The Effect of rolling reduction below recrystallization temperature of austenited on Ar_3 in Nb steel

Fig. 2.24 shows the relationship between the cumulative reduction below recrystallization temperature and Ar_3 for the case of unrecrystallized austenite , where data of

one pass rolling (750-850°C) and those 2-5 pass rolling at 900-800°C are included. The Ar_3 is raised drastically up to 40% reduction, beyond which it reachs a plateau. It is noted that Ar_3 is not dependent on the rolling temperature but dependent on the cumulative reduction. The raising of Ar_3 as a result of deformation is called strain induced transformation.

2.4 Effects of coiling temperature on mechanical property

The purpose of controlled coiling temperature of HSLA steels is to develop a fine, uniform ferrite grain size coupled with precipitation strengthening. The effectiveness of precipitation strengthening in HSLA steels is primarily affected by dissolution and precipitation behavior of microalloyed particle. Vanadium, at lower solution temperature, may contribute more to precipitation strengthening (72) , the solubility of vanadium carbide has been reported to dramatically higher than that of any other common microalloy precipitate such as TiC , VN, NbN and TiN (73). In general solubilities of microalloy nitrides are lower than those of corresponding carbides, especially for Ti and V (74). The solubilities of carbides and nitride such as TiC, NbC NbN, AIN and VN in austenite were reported similar (within an order of magnitude) , the solubility of VC was two or three orders of magnitude higher, and solubility of TiN was about four orders of magnitude less (75). This implies that TiN will precipitate first during the cooling process and dissolve last during the reheating process. In the Nb-Ti microalloyed system, Ti has been found to diffuse faster than Nb so that the nuclei of precipitates are rich in Ti and N and deficient in Nb and C. However , as the precipitates grow, Nb become the major diffusing element (76).

Equilibrium thermodynamics is believed to play a crucial role in determining the solubility of microalloying elements as a function of temperature and diffusion kinetics. Although practical mill processes are not at equilibrium, dissolution and precipitation can still follow the equilibrium sequence. First to make full use of microalloy precipitation hardening, the majority of pre-existing large (Nb, Ti) (C,N) particle formed during casting should be dissolved into solid solution. Hence, reheating temperature and time should be high and long enough , but not too high to promote complete dissolution and grain growth. Next , to maximize the precipitation hardening , these microalloys should precipitate as fine carbonitrides

during cooling. Hence controlling coiling temperature is necessary to achieve high strength by taking the advantage of both precipitation strengthening and grain refinement strengthening. Low coiling temperature can generally increase strength through grain refinement, but if coiling temperature is too low, precipitation can be suppressed (77) resulting in low strength. On the other hand if coiling temperature is too high, the precipitates will be few and large, and grain size will be large, which will also result in low strength. Thus, it is important to determine the optimum coiling temperature for maximum strengthening of Ti, Nb and V microalloyed HSLA steels.

2.4.1 Effect of alloying element on precipitation strengthening

There are three ways of increasing strength, grain refining, precipitation and transformation strengthening. The effect of Nb, Vand Ti on strength are shown in Fig. 2.25 (78)

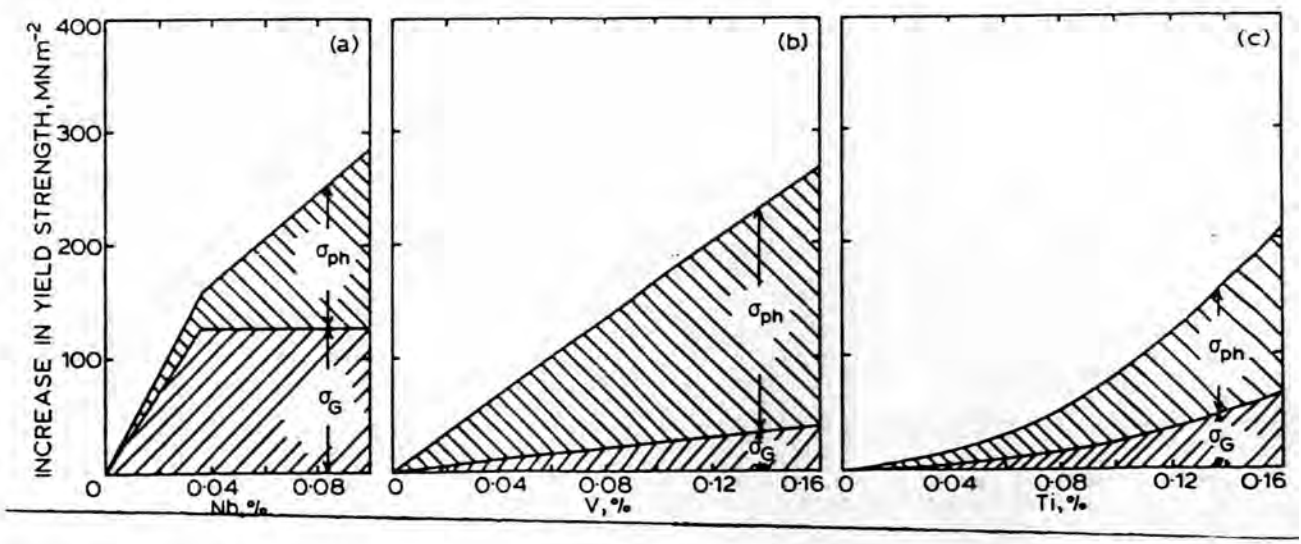

Fig. 2.25 Correlation between alloy content and increase in yield strength as result of grain refinement ($D\sigma_G$) and precipitation strengthening ($D\sigma_{ph}$).

Nb contributes to strength via both grain refining and precipitation particularly in low Nb content, major hardening is due to grain refinement. V causes a large increase strength through precipitation hardening. Ti cause a slight increase in strength via grain refinement and precipitation hardening.

2.4.2 *Effect of coiling temperature on mechanical properties and precipitate morphologies of Nb-Ti microalloyed steel*

C.R. Qing et al (79) has studied the effect of coiling temperature of 0.1%C , 0.24% Si, 1.2%Mn, 0.036% Nb and 0.036% Ti. Results of effect on ferrite grain size and mechanical properties are shown in Fig. 2.26

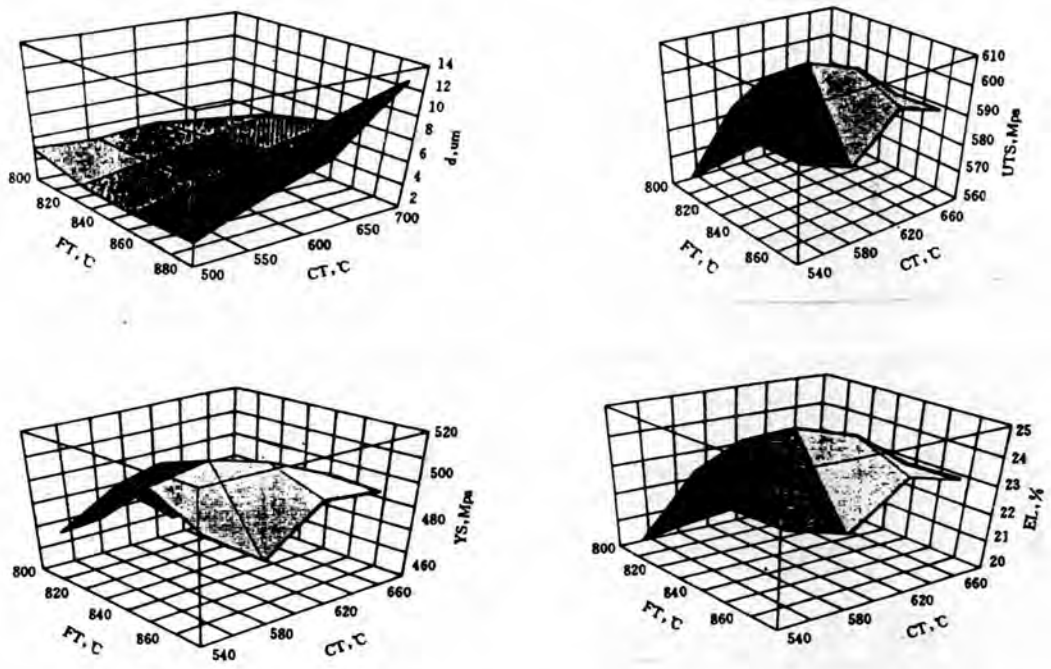

Fig. 2.26 Ferrite grain size and mechanical properties as a function of coiling temperatrue

As seen from Fig. 2.26 the ferrite grain size decrease with the decrease of finishing temperature and increases with the rising of coiling temperature. When coiling temperature is less than 650°C, the effect of coiling temperature on the grain size is not apparent. And the result of mechanical properties are in good agreement with changing trend in ferrite grain size.

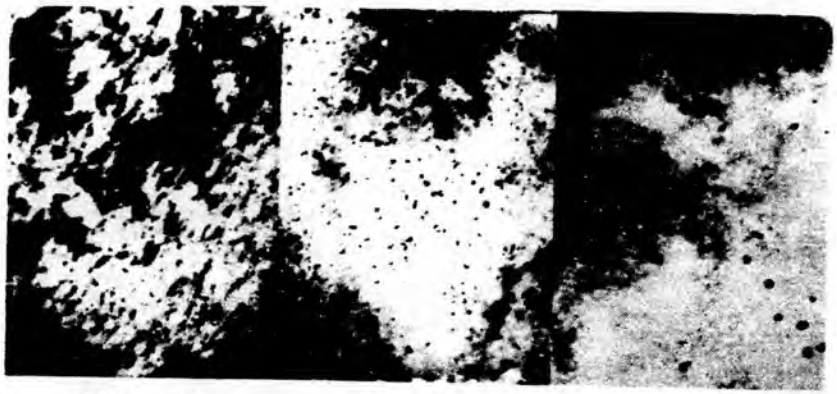

a)CT: 710℃ b)CT: 600℃ c)CT: 550℃

Fig. 2. 27 Precipitate morphologies at different coiling temperature

In Fig. 2.27 shows the precipitate morphologies at coiling temperature of 710°C , 600 °C and 550°C. It can be seen that more particles precipitate at the coiling temperature of 710°C and 600°C . However , at 600°C the particles in the ferrite are finer and more homogeneous. At the temperature of 550°C , the precipitate particle are less , coarser and uneven. The phenomena that the amount of precipitation as shown in Fig. 2.27 , decrease with the decline of coiling temperature is consistent with Kern (80).